

Air-Stable Molecular Semiconducting Iodosalts for Solar Cell Applications: Cs_2SnI_6 as a Hole Conductor

Byunghong Lee,^{†,‡} Constantinos C. Stoumpos,^{‡,§} Nanja Zhou,^{†,‡} Feng Hao,[§] Christos Malliakas,[§] Chen-Yu Yeh,[†] Tobin J. Marks,^{‡,§} Mercouri G. Kanatzidis,^{*,‡,§} and Robert P. H. Chang^{*,†,‡}

[†]Department of Materials Science and Engineering, Northwestern University, Evanston, Illinois 60208, United States

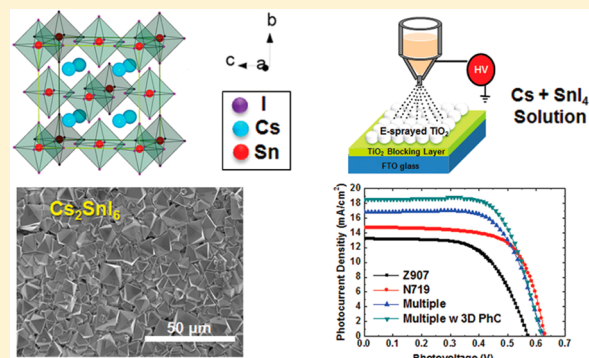
[‡]Argonne-Northwestern Solar Energy Research Center, Northwestern University, Evanston, Illinois 60208, United States

[§]Department of Chemistry, Northwestern University, Evanston, Illinois 60208, United States

[†]Department of Chemistry and Center of Nanoscience & Nanotechnology, National Chung Hsing University, Taichung 402, Taiwan

S Supporting Information

ABSTRACT: We introduce a new class of molecular iodosalt compounds for application in next-generation solar cells. Unlike tin-based perovskite compounds CsSnI_3 and $\text{CH}_3\text{NH}_3\text{SnI}_3$, which have Sn in the 2+ oxidation state and must be handled in an inert atmosphere when fabricating solar cells, the Sn in the molecular iodosalt compounds is in the 4+ oxidation state, making them stable in air and moisture. As an example, we demonstrate that, using Cs_2SnI_6 as a hole transporter, we can successfully fabricate in air a solid-state dye-sensitized solar cell (DSSC) with a mesoporous TiO_2 film. Doping Cs_2SnI_6 with additives helps to reduce the internal device resistance, improving cell efficiency. In this way, a Z907 DSSC delivers 4.7% of energy conversion efficiency. By using a more efficient mixture of porphyrin dyes, an efficiency near 8% with photon confinement has been achieved. This represents a significant step toward the realization of low-cost, stable, lead-free, and environmentally benign next-generation solid-state solar cells.



INTRODUCTION

During the past several years, there has been a surge of interest in the use of organic–inorganic hybrid perovskite compounds for applications in solar cells, primarily due to the high cell efficiencies obtained from these materials.^{1–6} The class of perovskite compounds under investigation has the ABX_3 structure. It consists of a network of corner-sharing BX_6 octahedra, where the B atom is a metal cation (typically Sn^{2+} or Pb^{2+}) and X is F^- , Cl^- , Br^- , or I^- . The A cation is selected to balance the total charge, and it can be Cs^+ , Rb^+ , K^+ , or a small molecular species.^{7,8} However, these perovskites exhibit long-term instabilities associated with phase transitions and ambient hydrolysis, and the presence of soluble lead compounds may limit widespread applications. Thus, to realize commercial applications of this technology, it is important to achieve analogous optical and photovoltaic performance using lead-free and air-stable organic–inorganic compounds for ambient processing. The purpose of this paper is to introduce an alternative and more stable class of molecular iodosalt compounds, A_2SnI_6 , where Sn is in the 4+ oxidation state. Note that the A_2SnI_6 compounds are not bona fide perovskites, in that they are molecular salts. They are soluble and do not suffer from many of the aforementioned disadvantages. The A_2SnI_6 compounds have a high-symmetry cubic structure with good air and moisture stability.⁹ In this article, we demonstrate

that Cs_2SnI_6 can serve as a hole-transporting material (HTM) in dye-sensitized solar cells (DSSCs). This is in contrast to organic HTMs, such as 2,2',7,7'-tetrakis(*N,N*-di-*p*-methoxyphenylamine)-9,9-spirobifluorene (spiro-OMeTAD), poly(triarylamines) (PTAAs), or tetrathiafulvalene derivatives (TTF-1).^{2,10,11} Using an electrospray (E-spray) technique to form the mesoporous nanostructured, layered TiO_2 anode, we demonstrate that the total cell internal resistance can be reduced by a factor of 2 as a result of better infiltration of Cs_2SnI_6 into the TiO_2 nanostructured layer. The effectiveness of the present cell design has been further evaluated using three types of dyes based on either Ru-bipyridine complexes N719 and Z907 or a mixture of N719 and Zn porphyrins YD2-o-C8 and RLC5 (see Supporting Information, SI-1). With process optimization, we have been able to obtain energy conversion efficiencies of 4.63%, 6.32%, and 6.94% with the respective dyes for cells with a thickness in the range of 5–7 μm . This is the first introduction of Cs_2SnI_6 (a new type of perovskite) as an air-stable HTM in a DSSC.

Received: August 18, 2014

Published: October 9, 2014

RESULTS

In this work, a solution-phase synthesis is used to prepare Cs_2SnI_6 (see Methods Section).¹² The structure of Cs_2SnI_6 is shown in Figure 1a. It is a defect variant of the AMX_3

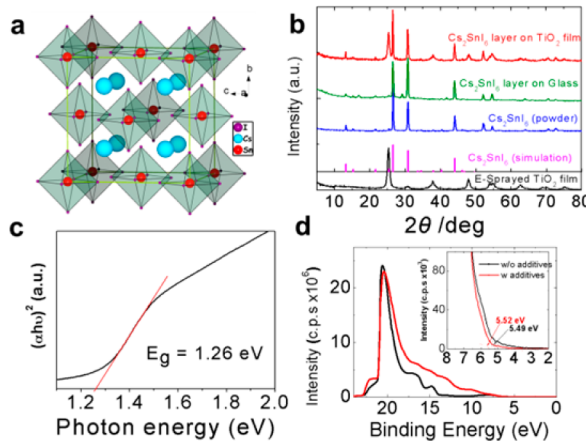


Figure 1. Crystal structure, XRD pattern, and optical properties of Cs_2SnI_6 . (a) Distorted three-dimensional structure of Cs_2SnI_6 at room temperature. In Cs_2SnI_6 , half of the octahedral Sn atoms are missing, creating discrete $[\text{SnI}_6]^{2-}$ octahedra. The compound is therefore a molecular salt and contains Sn^{4+} rather than Sn^{2+} in CsSnI_3 . This accounts for the stability of the material. (b) XRD spectra of the Cs_2SnI_6 at room temperature. The α -phase of the Cs_2SnI_6 powder structure is found and crystallizes in the cubic $Fm\bar{3}m$ space group with a lattice parameter of $11.6276(9)$ Å. (c) Assuming a direct band gap (E_g) for Cs_2SnI_6 , a Tauc plot indicates $E_g \approx 1.3$ eV. (d) UPS spectra from a sample of Cs_2SnI_6 . For the pristine Cs_2SnI_6 , the valence band energy (E_{vb}) is estimated as -5.49 eV with respect to vacuum level, whereas a similar $E_{vb} = -5.52$ eV is determined for Cs_2SnI_6 after doping with additives (see text).

perovskite structure type adopted by the CsSnI_3 , $\text{CH}_3\text{NH}_3\text{SnI}_3$, and $\text{CH}_3\text{NH}_3\text{PbI}_3$ compounds.^{13–15} In Cs_2SnI_6 , half of the octahedral Sn atoms are missing, creating discrete molecular $[\text{SnI}_6]^{2-}$ octahedra. The compound is therefore a molecular salt and contains Sn^{4+} rather than the extended Sn^{2+} -containing structure of CsSnI_3 . This accounts for the oxidative stability of the material. X-ray diffraction (XRD) measurements are shown in Figure 1b for both powder-synthesized and solution-processed Cs_2SnI_6 . The Cs_2SnI_6 at room temperature adopts the cubic $Fm\bar{3}m$ space group with a lattice parameter of $11.6276(9)$ Å.¹²

The presence of Cs_2SnI_6 on or in anatase electro-sprayed (E-sprayed) mesoporous TiO_2 films (identified by the (101) Bragg peak at $2\theta = 25.2^\circ$) is also confirmed by XRD. As shown in the optical absorption spectrum (Figure 1c), the band gap (E_g) of Cs_2SnI_6 is ~ 1.3 eV at room temperature. The measured charge-transport properties suggest a relatively low electrical resistivity of ~ 100 $\Omega\cdot\text{cm}$ for a virtually undoped sample prepared by annealing a pressed polycrystalline pellet of Cs_2SnI_6 at 200 °C. The carrier concentration (electrons) is found to be on the order of $\sim 1 \times 10^{14}$ cm^{-3} by room-temperature Hall effect measurements and was confirmed independently by the Seebeck coefficient ($S \approx -2.6 \times 10^3$ $\mu\text{V/K}$). Thus, the pristine bulk material behaves as an n-type semiconductor with a high electron mobility of 310 $\text{cm}^2/\text{V}\cdot\text{s}$. Remarkably, doping Cs_2SnI_6 with Sn^{2+} (as SnI_2) yields a material with a nearly identical carrier concentration ($\sim 1 \times 10^{14}$ cm^{-3}) but with the opposite sign—a p-type semiconductor, further confirmed by the

Seebeck data ($S \approx 1.9 \times 10^3$ $\mu\text{V/K}$). The hole mobility of the p-type Cs_2SnI_6 variant is lower than that of the n-type one, reaching a value of 42 $\text{cm}^2/\text{V}\cdot\text{s}$, corresponding to a significantly increased resistivity, 780 $\Omega\cdot\text{cm}$. Despite the reduction in mobility, p-type Cs_2SnI_6 still retains a sizable hole mobility, comparable to that of the $\text{CH}_3\text{NH}_3\text{PbI}_3$ perovskite.^{5,12} In addition, this behavior provides solid evidence of the ambipolar nature of Cs_2SnI_6 .

The above observations are in excellent agreement with our first-principles electronic band structure calculations (Figure 2a), which suggest Cs_2SnI_6 has a direct band gap of ~ 1.3 eV at

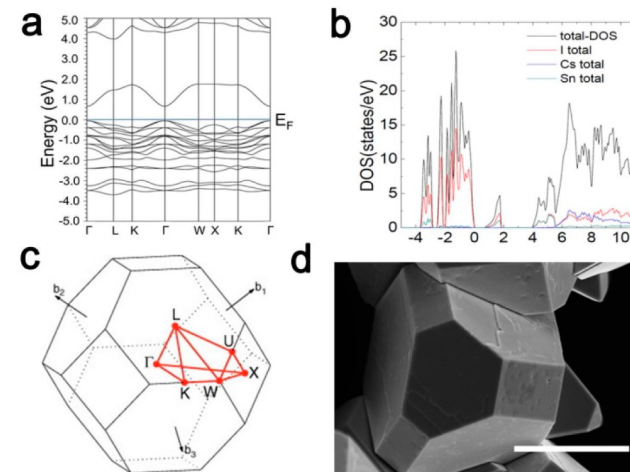


Figure 2. First-principles electronic band structure calculations. (a) The calculated electronic band structure at the Γ point. The valence and conduction bands are well dispersed in energy, for a molecular $[\text{SnI}_6]^{2-}$ salt compound, with ~ 1 and ~ 0.5 eV band widths, respectively. (b) Total DOS for Cs_2SnI_6 . (c) The calculated Brillouin zone of the fcc lattices,¹⁶ compared with (d) an SEM image of the typical crystal morphology of Cs_2SnI_6 . The scale bar is 40 μm .

the Γ point, comprising filled I-5p orbitals and empty hybrid I-6p/Sn-5s orbitals for the valence band maximum and conduction band minimum, respectively. The valence and conduction bands are surprisingly well dispersed in energy for a molecular $[\text{SnI}_6]^{2-}$ salt compound, with ~ 1 and ~ 0.5 eV band widths, respectively. Such a band configuration appears to justify the remarkably high electron and hole mobilities of Cs_2SnI_6 . Figure 2b–d shows, respectively, the total density of states (DOS) indicating the orbital contributions, the Brillouin zone of the fcc lattice, and an SEM image of the typical crystal morphology of Cs_2SnI_6 . Details on the calculations can be found in the Methods Section.

X-ray photoemission spectroscopy (XPS) measurements were performed on Cs_2SnI_6 -coated fluorine-doped tin oxide (FTO) substrates to assess the chemical composition and bonding states at the compound surface (Supporting Information, SI-2). Furthermore, ultraviolet photoemission spectroscopy (UPS) measurements were performed to determine the valence band maximum of Cs_2SnI_6 before and after doping with additives. Figure 1d shows the UPS spectra for the pristine Cs_2SnI_6 films and films after doping with additives, both prepared on ITO substrates. The binding energy was calibrated with respect to He I photon energy source (21.2 eV), and the valence band positions are determined from secondary electron cutoff (SECO) regions. For the pristine Cs_2SnI_6 , the valence band energy (E_{vb}) is estimated as -5.49 eV

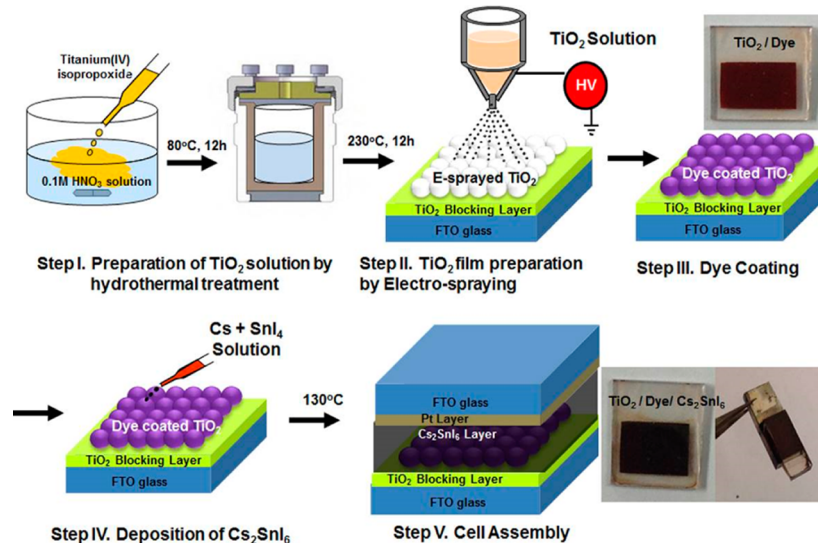


Figure 3. Illustrations showing fabrication procedure for Cs_2SnI_6 -based DSSCs. To obtain a continuous fluid jet during the electro-spraying, small-sized TiO_2 nanoparticles were first prepared by hydrothermal treatment. The hydrothermally treated TiO_2 solution was directly E-sprayed onto a FTO substrate. Following this, the electrodes were immersed into the dye. The Cs_2SnI_6 solution was spread in either one or two steps over the mesoporous TiO_2 layer containing the dye. This sample constitutes the anode of the cell. The cathode was fabricated by drop-casting the Cs_2SnI_6 solution with additives onto a FTO substrate with a very thin layer of sputtered Pt or Au. The final step is to press the two electrodes together to form the cell.¹⁸ This sandwiched device was placed on a hot plate ($\sim 130^\circ\text{C}$) and heated until the active film layer became virtually black in color (see Methods Section for details).

with respect to the vacuum level, whereas a similar $E_{\text{vb}} = -5.52$ eV is determined for Cs_2SnI_6 after inclusion of additives: lithium bis(trifluoromethylsulfonyl)imide (Li-TFSI) and 4-*tert*-butylpyridine (TBP) (see Methods Section for more details).

For the first step in our DSSC fabrication (Figure 3), we adopted an E-spray technique to fabricate a TiO_2 film containing mesoporous spheres (SPs) with a range of diameters between 100 and 500 nm, formed from nucleation and crystallization of 10 nm TiO_2 particles (Supporting Information, SI-3). Figure 4a,b shows SEM images of a distribution of mesoporous TiO_2 SPs in the anode electrode, under different magnifications. Figure 4c is a TEM image of the SPs; notice the

embedded crystalline nanoparticles (NPs) (see inset). This configuration gives increased internal surface area and also minimizes the internal series resistance of the electrode. The N_2 adsorption–desorption isotherms at 77 K of both TiO_2 SP and NP films (for conventional liquid DSSC fabrication) are shown in Figure 4d. The SP films show a type-IV isotherm as well as an increase in the adsorbed amount at high relative pressure, indicating the existence of mesopores in the sample.¹⁷ The surface area and pore sizes were calculated with the Brunauer–Emmett–Teller (BET) and Barrett–Joyner–Halenda (BJH) models.

The measured specific surface area of TiO_2 SPs is $\sim 114.0 \text{ m}^2/\text{g}$, ~ 2.1 -fold higher than that of TiO_2 NPs electrode (53.3 m^2/g). Furthermore, the total BJH mesopore volume and maximum pore radius are $0.723 \text{ cm}^3/\text{g}$ and 9.01 nm, respectively, while hydrothermal NP film shows the pore volume of $0.348 \text{ cm}^3/\text{g}$ and maximum pore radius of 1.06 nm.

With the available set of dye molecules used in this work, the band alignment is not optimal for Cs_2SnI_6 as a HTM. Nevertheless, we have made an attempt to improve the cell performance by optimizing the cell parameters, such as the fill factor (FF), the photocurrent (I), and the open-circuit voltage (V_{oc}). To this end we tried to (a) further improve the interpenetration of Cs_2SnI_6 into the mesoporous TiO_2 by varying its concentration during processing (however, we did not observe much overall improvement, as can be seen in Supporting Information, SI-4) and (b) understand the effect of using HTM additives such as Li-TFSI and TBP as previously described.^{18,19} The addition of Li salts and TBP in the HTM can improve the cell efficiency as a result of decreased resistance and reduced carrier recombination.^{20,21} In an effort to enhance the performance of Cs_2SnI_6 -based Z907 dye DSSCs, such Li-TFSI and TBP additives were also adopted in our study. From the electrochemical impedance spectroscopy measurements (see Supporting Information, SI-5), we analyzed the interfacial resistance of the Cs_2SnI_6 cell both with

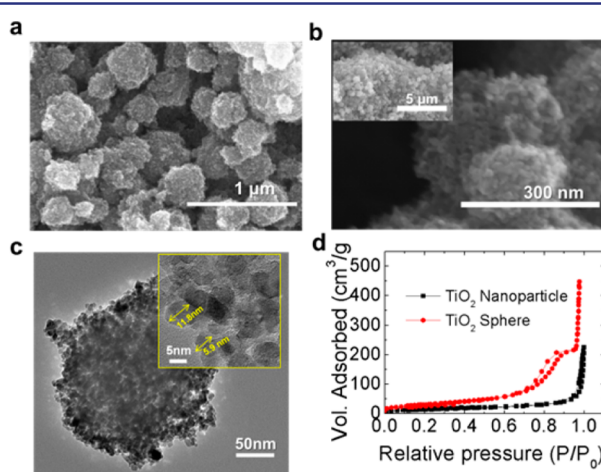


Figure 4. Morphology of E-sprayed TiO_2 spheres. (a,b) SEM images of a distribution of mesoporous TiO_2 spheres. E-sprayed TiO_2 films have mesoporous spherical shapes having a range of diameters, approximately 100–500 nm. (c) TEM image of the spheres which themselves are formed from crystallized ~ 10 nm particles (see inset). (d) N_2 adsorption–desorption isotherms of TiO_2 nanoparticles and spheres.

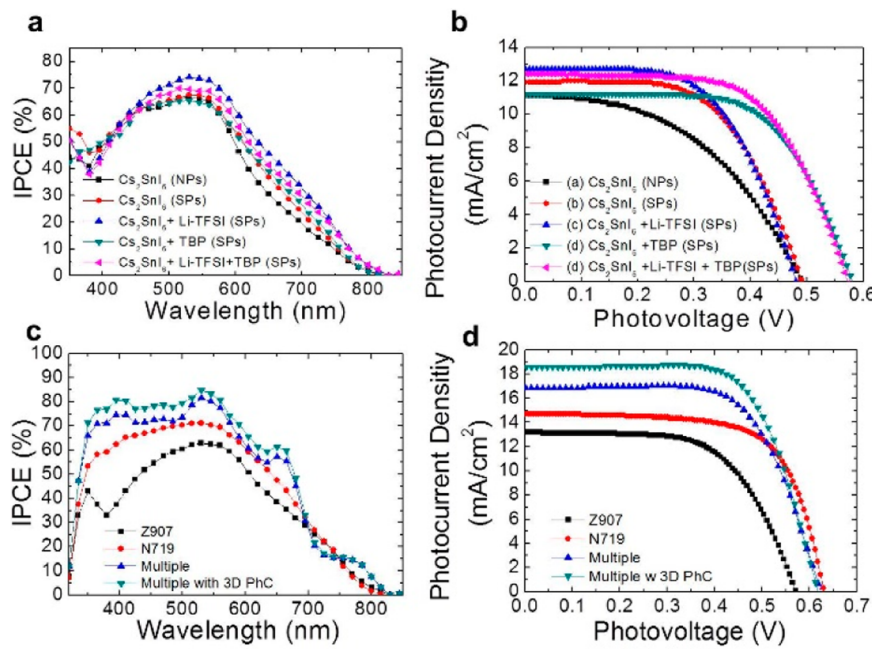


Figure 5. Solar cell performance of the Cs₂SnI₆-based solar cell. (a,b) IPCE spectra and *J*–*V* characteristics of Cs₂SnI₆ devices with different TiO₂ films and additives for a Z907 dye cell. (c,d) IPCE spectra and *J*–*V* characteristics of Cs₂SnI₆ devices with different sensitizers.

and without additives, following the procedures of Xia et al.¹⁸ Our results indicate that the overall interfacial recombination effects of additives on Cs₂SnI₆-based DSSCs are suppressed compared to the additives-free pristine Cs₂SnI₆-based DSSC by ~26.6%. This agrees well with the enhanced FF of the additives-containing solar cells.

Figure 5a shows the spectra of monochromatic incident photon-to-current conversion efficiencies (IPCEs) of our Cs₂SnI₆-based DSSCs. A comparative analysis of the quantum efficiency of a Z907 DSSC made from NPs and the E-sprayed SPs of TiO₂ using pristine Cs₂SnI₆ as HTMs was carried out. The overall IPCE value of the SPs-based DSSC is higher than that for the NPs-based DSSC.²² These results can be explained by the larger surface area and high porosity of TiO₂ SPs films, which have a positive effect on the HTM penetration and thus the DSSC photocurrent generation. In the case of cells containing the aforementioned HTM additives, the maximum IPCE exceeded 74% at 530 nm, ~10% higher than that for devices using Cs₂SnI₆ without additives at the same wavelength. This result clearly indicates that the additives play a crucial role in enhancing hole-transport characteristics. In Figure 5b and Supporting Information, Table S1, a significant improvement in energy conversion efficiency (ECE) is observed using additives (Li-TFSI and TBP) with Cs₂SnI₆: The best-performing device provides a ECE of ~4.63% ($V_{oc} = 0.571$ mV, $J_{sc} = 13.2$ mA/cm², FF = 61.3%) for a ~5 μm thick film.

To enhance the light-harvesting performance of the Cs₂SnI₆ cells, a “cocktail” of the N719 dye and other porphyrin dyes was explored. In the Supporting Information, Figure S1 (inset) illustrates the band alignment of the various components used in our cell preparation. The values for Z907 and N719 dyes are taken from the literature,^{23–25} while those for Cs₂SnI₆ were measured in this work. From the schematic band diagram, we anticipate that devices will perform better with N719 dye as compared to the Z907 dye, as will be verified below. From Figure S1, we see that while Z907 has an extended absorption onset compared to N719, its band alignment is not as ideal with

the Cs₂SnI₆ HTM. On the other hand, we find that greater care is required in fabricating N719 DSSCs. In a further investigation, a mixture of N719 with YD2-o-C8 and RLC5 dyes was used to extend the absorption spectrum (see Supporting Information, SI-1). The results of comparison using different dyes are shown in Figure 5c,d and Table 1 with their IPCE and *J*–*V* curves for an active layer thickness of ~5 μm. Note that a substantial increase in cell efficiency results from this wider-absorbing dye mixture.

Table 1. *J*–*V* Characteristics of Cs₂SnI₆-Coated Devices with Different Sensitizers, Containing Li-TFSI and TBP as Additives, with a TiO₂ Thickness of ~5 μm and a Total Cs₂SnI₆ Thickness of ~10 μm

cell	<i>J</i> – <i>V</i> characteristics			
	V_{oc} (V)	J_{sc} (mA/cm ²)	FF (%)	ECE (%)
Z907	0.571	13.2	61.3	4.63
N719	0.631	14.7	68.1	6.32
multiple	0.623	16.9	66.1	6.94
(with 3D PhC)	0.618	18.6	68.0	7.80

Photonic crystals were next used to confine those photons not absorbed by the cell in the ~600–800 nm range.²⁶ This increases the total ECE to nearly 8%. With respect to the stability of the cells, we first performed *J*–*V* measurements of a Z907 cell with and without additives at time zero (Figure 6a). Following that, long-term measurements of the Z907 cell with additives were carried out, as shown in Figure 6b, giving typical cell parameters (J_{sc} , ECE, FF, V_{oc}) as a function of time. After each data point the cell was left in the ambient environment. No accelerated stress test was performed. In comparison with Sn²⁺ perovskite compounds, the time stability is improved by at least an order of magnitude.²⁷

In conclusion, we have introduced a stable molecular iodosalt, Cs₂SnI₆, and demonstrated that it is a solution-processable semiconductor which can function as an efficient

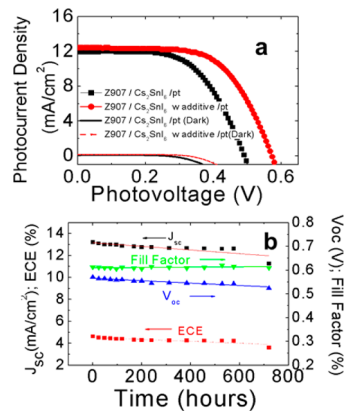


Figure 6. (a) J – V curve of a Z907 cell at time zero. (b) Long-term measurement of the parameters taken at regular intervals as a function of time.

DSSC HTM. This molecular salt is structurally related to the 113 perovskites such as the Sn²⁺ compound CsSnI₃ but has half of its Sn atoms missing. It has the advantage of being easy to process in solution and in ambient air. Using Cs₂SnI₆, we successfully fabricated DSSCs with a mesoporous TiO₂ spheres film prepared by an E-spray technique. Adding Li-TFSI and TBP to Cs₂SnI₆ reduces interfacial recombination and improves cell efficiency. In this way, a Z907/Cs₂SnI₆ DSSC delivers about 4.7% of energy conversion efficiency. Using a more efficient mixture of N719 with YD2-o-C8 and RLC5 dyes, the cell efficiency is increased to nearly 8% with photon confinement. It is significant that all fabrication here is in ambient air, which represents an important step toward the realization of low-cost, lead-free, and environmentally benign next-generation solid-state solar cells with high-efficiency.

METHODS SECTION

Synthesis of Cs₂SnI₆. A 100 mL beaker was charged with a mixture of aqueous HI (20 mL, 7.58 M) that was next carefully mixed with Cs₂CO₃ (3.258 g, 10 mmol) to afford a concentrated acidic solution of CsI. In a separate 50 mL beaker, SnI₄ (3.132 g, 5 mmol) was dissolved in 10 mL of warm absolute EtOH to afford a clear orange solution. Addition of the alcoholic SnI₄ solution to the aqueous CsI solution under vigorous stirring led to spontaneous precipitation of a fine black powder. The mixture was stirred for a further 10 min to ensure completion of the reaction, after which the solid was filtered off and washed copiously with absolute EtOH. The yield of the reaction is quantitative, including only manipulative losses (~5.5 g of Cs₂SnI₆ can be isolated). Black truncated octahedral crystals of Cs₂SnI₆ can be obtained by liquid diffusion of the alcoholic SnI₄ solution into the aqueous CsI solution at low concentrations. The compound is air- and moisture-stable at room temperature.

Solar Cell Fabrication Process. Following the sequence shown in Figure 3, a TiO₂ NP solution was hydrothermally prepared according to the method described in the Supporting Information, SI-3. The aqueous solvent was replaced by ethanol without any added organic binder. The replaced TiO₂ solution was directly E-sprayed onto a FTO substrate (Pilkington, TEC 8 glass), the surface of which was pretreated with a dense blocking layer of TiO₂, using a 30 mM titanium diisopropoxide bis(acetylacetone) solution (Aldrich) in butanol, followed by annealing at 500 °C. After E-spray, the as-prepared TiO₂ mesoporous film-coated anode electrode was heated to 500 °C from room temperature in 30 min. A post-treatment was applied as described in the literature.²⁸ Following this, the anode electrodes were immersed into dye-containing solution. For the case of Z907 dye, the electrodes were immersed into 3.0 × 10⁻⁴ M *cis*-bis(isothiocyanato)(2,2'-bipyridyl-4,4'-dicarboxylato)(2,2'-bipyridyl-

4,4'-dinonyl)ruthenium(II) (known as Z-907, Aldrich) in dichlorobenzene for 12 h and spun at 2500 rpm for 45 s. For the case of N719 dye, the electrodes were immersed into 3.0 × 10⁻⁴ M *cis*-bis(isothiocyanato)(2,2'-bipyridyl-4,4'-dicarboxylato)(2,2'-bipyridyl-4,4'-dinonyl)ruthenium(II) (known as N719, Aldrich) in 1,2-dichlorobenzene for 12 h and spinning at 2500 rpm for 45 s to ensure good contact. For other dyes, similar procedures were used. (For details, please see Supporting Information, SI-1.)

To apply crystallites of Cs₂SnI₆ as HTM in a DSSC, the compound was completely dissolved in *N,N*-dimethylformamide (DMF) at room temperature. For a concentration study, 50 mg of Cs₂SnI₆ was dissolved in 1 mL of DMF. For additive (doping) studies, TBP was added to the Cs₂SnI₆ solution with a volume-to-mass ratio of 1:26 μL/mg TBP:Cs₂SnI₆. A stock solution was prepared by dissolving 170 mg of Li-TFSI in 1 mL of acetonitrile, and then 37.5 μL of this mixture was introduced as an additive.¹⁹ The HTM solution was lightly spread over the dye-containing mesoporous TiO₂ by dropping Cs₂SnI₆ solution. The sample was then heated at 130 °C for 20 s in ambient atmosphere. This sample constitutes the anode-electrode of the cell. The cathode-electrode was fabricated by drop-casting the Cs₂SnI₆ solution with additives onto a FTO substrate with a very thin layer of sputtered Pt or Au. The final step was to press the two electrodes together to form the cell. This sandwiched device was placed on a hot plate (~130 °C) and heated for a few minutes until the active film layer became virtually black in color and dry. A schematic illustrating this sequence of processing is shown in Figure 3 (with details in Supporting Information, SI-3).

Solution Synthesis of Cs₂SnI₆ and Fabrication. A 100 mL two-necked round-bottom flask was charged with a mixture of aqueous HI (6.8 mL, 7.58 M) and aqueous H₃PO₂ (1.7 mL, 9.14 M). The liquid was degassed by passing a stream of nitrogen through it for 1 min and keeping it under a nitrogen atmosphere throughout the experiment. SnI₂ (372 mg, 1 mmol) was dissolved in the mixture upon heating the flask to 120 °C using an oil bath, under constant magnetic stirring, forming a bright yellow solution. To the hot yellow solution was added solid CsI (260 mg, 1 mmol). Two minutes after the addition, yellow needle-shaped crystals started to precipitate. The precipitate was dissolved by adding 10 mL of acetone, producing a dark red solution. After 5 min, the stirring was discontinued, and the solution was left to cool to room temperature. Black truncated octahedral (14 faces) crystals were formed upon standing. The crystals were left to grow inside the mother liquor for another 24 h under a nitrogen atmosphere before being filtered and washed with degassed EtOH, with a yield of 80–90%. The compound is air- and water-stable. Cs₂SnI₆ was completely dissolved in DMF by stirring the solution. For the concentration study, Cs₂SnI₆ was prepared by dissolving 50 mg of Cs₂SnI₆ in 1 mL of DMF. The HTM solutions were lightly spread over the dyed surface by drop-coating and left for 5 min. These samples coated with HTM were heated at 110 °C, and the procedure was repeated about three times. A Pt-sputtered conducting tin oxide glass plate was pressed into the Cs₂SnI₆ surface to serve as the back contact.¹⁸ These sandwiched devices were placed on a hot plate (~110 °C) and heated for a few minutes until the film could be visually recognized by the black color.

Sequential Deposition. To coat different thicknesses of Cs₂SnI₆ layers, a novel two-step coating process (E-spraying technique) has been developed in our laboratory. At the first step, a CsI solution was prepared by dissolving 1 g of CsI powder (Aldrich, 99.9%) in 50 mL of DMF or water. After stirring, the solutions were loaded into a plastic syringe equipped with a 25-gauge stainless steel needle. The spinning rate was controlled by a syringe pump (KD Scientific model 220) at 25 μL/min. An electric field of 12–15 kV was applied between a metal orifice and the FTO substrate at a distance of 10 cm by a power supply (Bertan Series 205B). The duration of E-spraying controls the thickness of CsI layers, and this film was heated at 130 °C for 10 min in ambient atmosphere.

In the second step, a solution of tin(IV) iodide (SnI₄) in ethanol (0.1 g/mL) was introduced into the CsI layer by drop-casting. The drop process was repeated several times until the color of the covered

CsI layer changed to black, indicating the formation of the Cs_2SnI_6 phase. This black film was heated in air at 110 °C for 5 min.

Photovoltaic Characterization. A Newport-Oriel IQE-200 ACDC was used to measure incident photon-to-charge carrier efficiency (IPCE). The DSSC devices were evaluated under 100 mW/cm² AM1.5G simulated sunlight with a class A solar cell analyzer (Spectra Nova Tech.). A silicon solar cell fitted with a KG3 filter, tested and certified by the National Renewable Energy Laboratory (NREL), was used for calibration. The KG3 filter accounts for the different light absorption between the dye-sensitized solar cell and the silicon solar cell, and it ensures that the spectral mismatch correction factor approaches unity. The electrochemical impedance results were measured under the same light illumination with an impedance analyzer (Solartron 1260) and a potentiostat (Solartron 1287) when the device was applied at its V_{oc} . An additional low-amplitude modulation sinusoidal voltage of 10 mV rms was also applied between the anode and cathode of a device over the frequency range of 0.05–150 kHz.

Band Gap Measurements. Optical diffuse reflectance measurements were performed at room temperature using a Shimadzu UV-3600 PC spectrometer operating in the 200–2500 nm region. The reflectance versus wavelength data generated were used to estimate the band gap of the material by converting reflectance to absorption data according to the Kubelka–Munk equation: $\alpha/S = (1 - R)^2/2R$, where R is the reflectance and α and S are the absorption and scattering coefficients, respectively.^{13,19}

Charge-Transport Property Characterization. Rectangular, cold-pressed pellets annealed at 200 °C under 10⁻⁴ mbar vacuum were used for the measurements. Resistivity, Seebeck coefficient, and Hall effect measurements were performed at room temperature using a homemade setup as described previously.⁸

First-Principles Band Structure Calculations. Electronic structure calculations were performed using the self-consistent full-potential linearized augmented plane wave method (LAPW)²⁹ within density functional theory (DFT),^{30,31} using the generalized gradient approximation (GGA) of Perdew, Burke, and Ernzerhof³² for the exchange and correlation potential. The values of the atomic radii were taken to be 2.5 a.u. for Cs, Sn, and I atoms, where a.u. is the atomic unit (0.529 Å). Convergence of the self-consistent iterations was performed for 286k points inside the irreducible Brillouin zone to within 0.0001 Ry, with a cutoff of −6.0 Ry between the valence and the core states. Scalar relativistic corrections were included, and a spin–orbit interaction was incorporated using a second variational procedure.³³ Band gap correction was included using the modified Becke–Johnson exchange potential.³⁴ The calculations were performed using the WIEN2k program.³⁵

XPS and UPS Measurements. XPS (Omicron ESCA Probe) surface measurement was performed on Cs_2SnI_6 -coated FTO substrates. The samples were sputtered with an Ar⁺ gun at 3000 eV for 5 s to remove surface contaminants. UPS spectra were recorded on a Thermo Scientific ESCALAB 250Xi system at a base pressure of 8×10^{-10} mbar (UHV), using a 21.2 eV He I source at a pass energy of 2 eV and an energy step size of 0.05 eV. The instrument was calibrated with a standard gold electrode, and a −10 V sample bias was applied to determine the SECO for all samples by curve fitting. Three measurements were averaged for each sample.

ASSOCIATED CONTENT

Supporting Information

Additional characterizations on material and device properties. This material is available free of charge via the Internet at <http://pubs.acs.org>.

AUTHOR INFORMATION

Corresponding Authors

m-kanatzidis@northwestern.edu
r-chang@northwestern.edu

Notes

The authors declare no competing financial interest.

ACKNOWLEDGMENTS

This research was supported as part of the Argonne–Northwestern Solar Energy Research Center (ANSER), an Energy Frontier Research Center funded by the U.S. Department of Energy, Office of Science, Office of Basic Energy Sciences (award no. DE-SC0001059), and Institute for Sustainability and Energy at Northwestern (ISEN). We thank the NSF-MRSEC program through the Northwestern University Materials Research Science and Engineering Center for characterization facilities (DMR-1121262). XRD measurements were performed at the J. B. Cohen X-Ray Diffraction Facility, supported by the MRSEC program of the National Science Foundation (DMR-1121262) at the Materials Research Center of Northwestern University. Electron microscopy and elemental analysis were carried out at the Electron Probe Instrumentation Center (EPIC) at Northwestern University.

REFERENCES

- (1) Lee, M. M.; Teuscher, J.; Miyasaka, T.; Murakami, T. N.; Snaith, H. J. *Science* **2012**, *338*, 643.
- (2) Burschka, J.; Pellet, N.; Moon, S.-J.; Humphry-Baker, R.; Gao, P.; Nazeeruddin, M. K.; Grätzel, M. *Nature* **2013**, *499*, 316.
- (3) Liu, M.; Johnston, M. B.; Snaith, H. J. *Nature* **2013**, *501*, 395.
- (4) Noh, J. H.; Im, S. H.; Heo, J. H.; Mandal, T. N.; Seok, S. I. *Nano Lett.* **2013**, *13*, 1764.
- (5) Ogomi, Y.; Morita, A.; Tsukamoto, S.; Saitho, T.; Fujikawa, N.; Shen, Q.; Toyoda, T.; Yoshino, K.; Pandey, S. S.; Ma, T.; Hayase, S. *J. Phys. Chem. Lett.* **2014**, *5*, 1004.
- (6) Hao, F.; Stoumpos, C. C.; Chang, R. P. H.; Kanatzidis, M. G. *J. Am. Chem. Soc.* **2014**, *136*, 8094.
- (7) Borriello, I.; Cantele, G.; Ninno, D. *Phys. Rev. B* **2008**, *77*, 235214.
- (8) Mitzi, D. B. *Progress in Inorganic Chemistry*; John Wiley & Sons, Inc.: New York, 2007; p 1.
- (9) Brik, M. G.; Kityk, I. V. *J. Phys. Chem. Solids* **2011**, *72*, 1256.
- (10) Jeon, N. J.; Noh, J. H.; Kim, Y. C.; Yang, W. S.; Ryu, S.; Seok, S. I. *Nat. Mater.* **2014**, *13*, 897.
- (11) Liu, J.; Yongzhen, W.; Qin, C.; Yang, X.; Yasuda, T.; Islam, A.; Zhang, K.; Peng, W.; Han, L.; Chen, W. *Energy Environ. Sci.* **2014**, *7*, 2963.
- (12) Stoumpos, C. C.; Malliakas, C. D.; Kanatzidis, M. G. *Inorg. Chem.* **2013**, *52*, 9019.
- (13) Chung, I.; Song, J.-H.; Im, J.; Androulakis, J.; Malliakas, C. D.; Li, H.; Freeman, A. J.; Kenney, J. T.; Kanatzidis, M. G. *J. Am. Chem. Soc.* **2012**, *134*, 8579.
- (14) Hao, F.; Stoumpos, C. C.; Cao, D. H.; Chang, R. P. H.; Kanatzidis, M. G. *Nat. Photon.* **2014**, *8*, 489.
- (15) Mosconi, E.; Amat, A.; Nazeeruddin, M. K.; Grätzel, M.; De Angelis, F. *J. Phys. Chem. C* **2013**, *117*, 13902.
- (16) Setyawan, W.; Curtarolo, S. *Comput. Mater. Sci.* **2010**, *49*, 299.
- (17) Kruk, M.; Jaroniec, M. *Chem. Mater.* **2001**, *13*, 3169.
- (18) Xia, J.; Masaki, N.; Lira-Cantu, M.; Kim, Y.; Jiang, K.; Yanagida, S. *J. Am. Chem. Soc.* **2008**, *130*, 1258.
- (19) Noh, J. H.; Jeon, N. J.; Choi, Y. C.; Nazeeruddin, M. K.; Grätzel, M.; Seok, S. I. *J. Mater. Chem. A* **2013**, *1*, 11842.
- (20) Krüger, J.; Plass, R.; Cevey, L.; Piccirelli, M.; Grätzel, M.; Bach, U. *Appl. Phys. Lett.* **2001**, *79*, 2085.
- (21) Snaith, H. J.; Grätzel, M. *Appl. Phys. Lett.* **2006**, *89*.
- (22) Park, N. G.; van de Lagemaat, J.; Frank, A. J. *J. Phys. Chem. B* **2000**, *104*, 8989.
- (23) Ravirajan, P.; Peiró, A. M.; Nazeeruddin, M. K.; Graetzel, M.; Bradley, D. D. C.; Durrant, J. R.; Nelson, J. *J. Phys. Chem. B* **2006**, *110*, 7635.

- (24) Daeneke, T.; Kwon, T.-H.; Holmes, A. B.; Duffy, N. W.; Bach, U.; Spiccia, L. *Nat. Chem.* **2011**, *3*, 211.
- (25) Chung, I.; Lee, B.; He, J.; Chang, R. P. H.; Kanatzidis, M. G. *Nature* **2012**, *485*, 486.
- (26) Lee, B.; Hwang, D.-K.; Guo, P.; Ho, S.-T.; Buchholtz, D. B.; Wang, C.-Y.; Chang, R. P. H. *J. Phys. Chem. B* **2010**, *114*, 14582.
- (27) Zhou, H.; Chen, Q.; Li, G.; Luo, S.; Song, T.-b.; Duan, H.-S.; Hong, Z.; You, J.; Liu, Y.; Yang, Y. *Science* **2014**, *345*, 542.
- (28) Lee, B. H.; Song, M. Y.; Jang, S.-Y.; Jo, S. M.; Kwak, S.-Y.; Kim, D. Y. *J. Phys. Chem. C* **2009**, *113*, 21453.
- (29) Singh, D. *Planewaves, Pseudopotentials, and the LAPW method*; Kluwer Academic: Boston, MA, 1994.
- (30) Kohn, W.; Sham, L. J. *Phys. Rev.* **1965**, *140*, A1133.
- (31) Hohenberg, P.; Kohn, W. *Phys. Rev.* **1964**, *136*, B864.
- (32) Perdew, J. P.; Burke, K.; Ernzerhof, M. *Phys. Rev. Lett.* **1996**, *77*, 3865.
- (33) Koelling, D. D.; Harmon, B. N. *J. Phys. C: Solid State Phys.* **1977**, *10*, 3107.
- (34) Tran, F.; Blaha, P. *Phys. Rev. Lett.* **2009**, *102*, 226401.
- (35) Blaha, P.; Schwarz, K.; Madsen, G. K. H.; Kvasnicka, D.; Luitz, J. *WIEN2k, An Augmented Plane Wave + Local Orbitals Program for Calculating Crystal Properties*; Techn. Universität Wien: Wien, Austria, 2001.